ARTICLE

Inversion Domain Boundaries in GaN Wires Revealed by Coherent Bragg Imaging

Stéphane Labat,[*,†] Marie-Ingrid Richard,[†,‡] Maxime Dupraz,[§,∥] Marc Gailhanou,[†] Guillaume Beutier,[§,∥] Marc Verdier,[§,∥] Francesca Mastropietro,[†] Thomas W. Cornelius,[†] Tobias U. Schülli,[‡] Joël Eymery,[⊥,#] and Olivier Thomas[†]

[†]IM2NP UMR 7334, Aix Marseille Université, CNRS, Université de Toulon, F-13397 Marseille, France, [‡]ID01 ESRF, F-38043 Grenoble, France, [§]Université Grenoble Alpes, SIMAP, F-38000 Grenoble, France, [∥]CNRS, SIMAP, F-38000 Grenoble, France, [⊥]Université Grenoble Alpes, F-38000 Grenoble, France, and [#]"Nanophysique et Semiconducteurs" Group, CEA, INAC-SP2M, F-38000 Grenoble, France

ABSTRACT Interfaces between polarity domains in nitride semiconductors, the so-called Inversion Domain Boundaries (IDB), have been widely described, both theoretically and experimentally, as perfect interfaces (without dislocations and vacancies). Although ideal planar IDBs are well documented, the understanding of their configurations and interactions inside crystals relies on perfect-interface assumptions. Here, we report on the microscopic configuration of IDBs inside n-doped gallium nitride wires revealed by coherent X-ray Bragg imaging. Complex IDB configurations are evidenced with 6 nm resolution and the absolute polarity of each domain is unambiguously identified. Picoscale displacements along and across the wire are directly extracted from several Bragg reflections using phase retrieval algorithms, revealing rigid relative displacements of the domains and the absence of microscopic strain away from the IDBs. More generally, this method offers an accurate inner view of the displacements and strain of interacting defects inside small crystals that may alter optoelectronic properties of semiconductor devices.

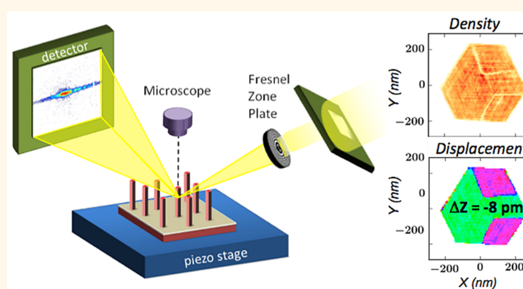

KEYWORDS: GaN wires · inversion domain boundary · coherent X-ray Bragg imaging · displacement field

The physical properties of crystals are strongly affected by the presence of defects: dislocations, stacking faults and twins have a prominent role in the mechanical behavior, vacancies are crucial in the diffusion process and electrical, and optical properties are widely affected by defects too.[1] The detailed knowledge of defects distribution in crystals is thus a prerequisite for understanding how physical properties are affected. For many years, methods based on transmission electron microscopy (TEM) have been unchallenged for investigating defects in crystals and have provided numerous essential results.[2−6] But recently, a new lensless imaging technique using coherent X-ray diffraction has emerged, which is able to determine the atomic displacement field in a crystal from the measurement of Bragg reflections.[7] This technique is called Coherent Bragg Imaging (CBI). Up to now, it has been mainly used, however, for imaging perfect crystals with very small strain.[7−10] Very few works use it for materials containing defects.[11−13]

Here, we report on the first study of the displacement field induced by several Inversion Domain Boundaries in Gallium Nitride (GaN) wires with a spatial resolution better than 10 nm and a displacement accuracy of a few picometres. Nitride materials are studied intensively and their growth mastering has opened the way to blue-light emission[14] and power devices applications. Since defects in GaN wires are a key issue,[15] such results give new insights into the optoelectronic properties of nitride semiconductors.

RESULTS AND DISCUSSION

The GaN wires of this study were grown by Metal Organic Vapor Phase Epitaxy (MOVPE) on a *c*-oriented sapphire substrate. A sample with a low wire density was prepared

* Address correspondence to stephane.labat@im2np.fr.

Received for review June 24, 2015 and accepted August 31, 2015.

Published online August 31, 2015
10.1021/acsnano.5b03857

© 2015 American Chemical Society

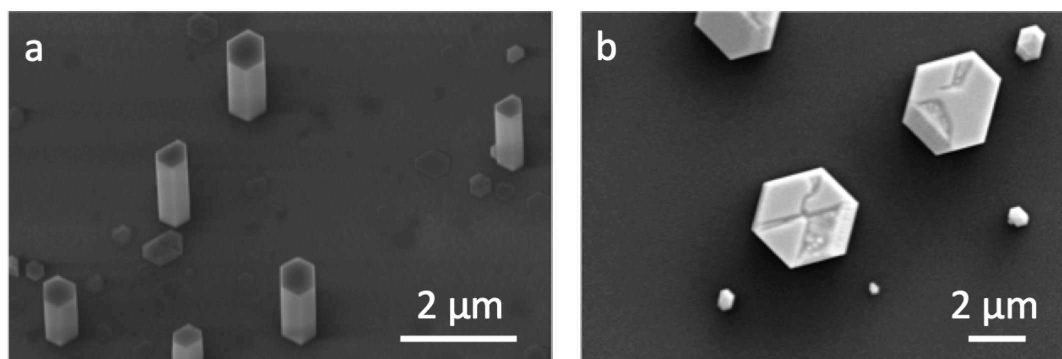

Figure 1. Scanning electron microscopy images of GaN wires obtained by MOVPE. (a) A 25°-view taken at the center of the wafer showing single crystal wires and (b) top view taken at the wafer edge for a sample etched under H_2 carrier gas to underline polarity inversion domain boundaries. The growth conditions (mostly flows and materials supply) are changed in the 2 mm outer edges.

in order to ease the individual analysis with the micro-focused X-ray beam: specific surface annealings and growth conditions (detailed in the Methods section) promote the 'vertical' growth (*i.e.*, perpendicular to the surface of the substrate) of hexagonal wires with average diameter of 600 nm and length of 3−5 μm (Figure 1a).

They have their *c*-axis parallel or antiparallel to the growth axis and smooth lateral $\{1\bar{1}0\}$*m*-plane facets. The wires are in epitaxial relationship with the sapphire as confirmed by grazing incidence X-ray and electron diffraction: $[1\bar{1}0]_{GaN}//[0\bar{1}0]_{Al203}$ and $[00\bar{1}]_{GaN}//[001]_{Al203}$ with twist and tilt misorientations of less than half a degree.[16] TEM studies have shown that "defect-free wires" are single crystalline with a flat top surface and have no extended defects along the length, except for threading dislocations nucleated at the lattice mismatched interface. These dislocations are usually bent to the sidewall surface along a distance of the order of magnitude of the diameter.[5,17] Polarity in non-centrosymmetric wurtzite crystal is defined with standard notations: the bond pointing from the Ga cation to the N anion defines the polar axis *c* labeled [001] also called Ga-polar orientation. Within the selected growth conditions, the wires are mostly N-polar oriented, *i.e.*, along −*c* axis. Nevertheless, IDBs separating +*c* and −*c* crystal orientation domains have been observed in the core of guided wires close to the holes of patterned masks.[5,18] The lateral overgrowth tends to favor the occurrence of IDBs nucleating on the surface defects of the SiN_x seed layer.[19] In this paper, we select "defective" wires close to the wafer edge in order to increase the probability of occurrence of IDB defects and to benefit from an even lower wire density. This defective character has been checked by etching a sample at the end of the growth under H_2 to reveal selectively the −*c* and +*c* orientation domains (note that similar results can be obtained *ex situ* by wet KOH solutions[20]): under H_2 carrier gas, −*c* (nitrogen-terminated) GaN surface stays flat, whereas the +*c* (gallium-terminated) surface is roughened and exhibits small faceted pyramids. This procedure is demonstrated in

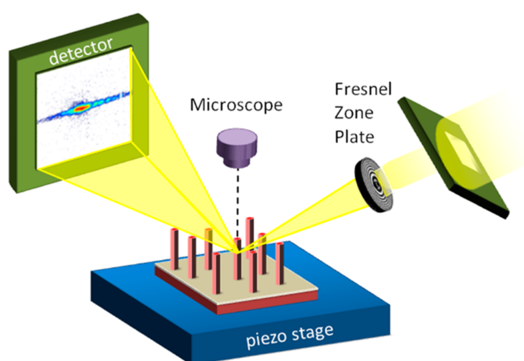

Figure 2. Sketch of the experimental setup for coherent X-ray Bragg imaging.

Figure 1b. IDBs are clearly observed and show complex structures separating flat (−*c*) and rough (+*c*) surfaces. Note that facets can be visible at some wire edges. This faceting provides also a signature of +*c* GaN growth as evidenced by previous TEM studies.[5]

The CBI technique was used to investigate the arrangement of the IDBs inside the GaN wires and the displacement field generated by these defects. The very good epitaxial relationship of the wires with the substrate eases the otherwise tedious alignment procedure of a known wire with the microfocused X-ray beam (Figure 2).

When a crystal is fully illuminated by a coherent X-ray beam, the scattered waves from all parts of the sample interfere in the diffraction pattern. The intensity scattered by the sample is measured in far field and a real space image of the sample may be reconstructed from the intensity pattern thanks to phase retrieval algorithms. When the intensity pattern is measured close to a Bragg peak, a complex-valued image of the sample (named $\rho(\mathbf{r})$) is retrieved, which is related to the structure factor $F(\mathbf{G,r})$ and the displacement field $\mathbf{U}(\mathbf{r})$ by the expression:

$$\rho(\mathbf{r}) = F(\mathbf{G}, \mathbf{r})\, e^{-i2\pi\mathbf{G}.\mathbf{U}(\mathbf{r})} \quad (1)$$

where **G** corresponds to the scattering vector of the Bragg Peak. Note that the sign convention used to

describe the plane wave e^{ikr} implies a minus sign in the Fourier transform of eq 1. The spatial resolution or pixel size of the reconstructed image of the object is inversely proportional to the extension of the intensity measurements around the Bragg peak. Extended diffraction pattern measurements provide small pixel sizes in the reconstructed sample images. Because of the steep decrease of intensity away from the Bragg peaks, the pixel size in the sample image is rarely smaller than 10 nm. For the sake of clarity, the modulus $M(\mathbf{r})$ and phase $\phi(\mathbf{r})$ of the reconstructed object will be displayed in two separate images. From eq 1, $M(\mathbf{r})$ and $\phi(\mathbf{r})$ can be written as

$$M(\mathbf{r}) = |F(\mathbf{G}, \mathbf{r})| \quad \text{and} \quad \phi(\mathbf{r}) = \psi_F(\mathbf{G}, \mathbf{r}) - 2\pi\mathbf{G}.\mathbf{U}(\mathbf{r}) \quad (2)$$

where ψ_F corresponds to the phase of the complex structure factor $F(\mathbf{G},\mathbf{r})$. In the case of GaN wires containing inversion domains, the same moduli are expected for the two types of domain, but different phases will be observed including the effects of the structure factors and the displacement field. Thus, one expects a homogeneous modulus map $M(\mathbf{r})$ and an inhomogeneous phase map $\phi(\mathbf{r})$. Each Bragg peak is sensitive to the displacement field $\mathbf{U}(\mathbf{r})$ projected onto the scattering vector $\mathbf{G}$, *i.e.*, $\mathbf{G}.\mathbf{U}(\mathbf{r})$. To extract the full displacement vector field $\mathbf{U}(\mathbf{r})$, at least three noncoplanar Bragg peaks are needed. In this work, we measured five Bragg peaks: 004, 014, 104, 112, and 203. The redundancy is expected to improve the reliability of the retrieved vector field $\mathbf{U}(\mathbf{r})$. The intensity measurements were done while illuminating a slab (~400 nm thick) at mid-height of the wire. Each of the five diffraction patterns was measured in three dimensions by recording a stack of frames of an area detector while rocking the sample across the reflection. In all three-dimensional diffraction patterns, the measured intensity is concentrated in an (h,k)-plane perpendicular to the l-axis. This means that the inner structure of the measured slab is constant along the wire axis. 2D intensity maps were thus extracted from the 3D data sets in order to reconstruct a 2D image of the sample (Figure 3a). The latter is therefore a projection of the measured slab along the c-axis, which provides a good image of the inner structure in this translation-invariant sample.

In all five diffraction patterns, the 6 streaks observed along directions separated by an angle of 60° clearly demonstrate the hexagonal shape of the wire. Each diffraction pattern was used independently to reconstruct an image of the inner structure of the wire with different displacement field components. The sample is reconstructed with a pixel size of 6×6 nm^2 because of the extent of the measured intensity in the reciprocal space. Phase retrieval of the diffraction data was carried out using standard algorithms[21,22] based on Fourier transforms going back and forth between the direct space (sample image) and the reciprocal space (diffraction patterns).

The reconstruction procedure (see Methods and Supporting Information S1) is carried out a thousand times with random initial phases for each diffraction pattern. Two criteria were used to identify the best reconstructions: the agreement with the measured intensity and the homogeneity of the modulus map. The best solutions, which fulfill these two criteria, are used to determine the accuracy of the results (see Supporting Information S1). Then, we are still left with two solutions, $\rho(\mathbf{r})$ and $\rho^*(-\mathbf{r})$, which fulfill equally the two criteria (Figure 4).

For this specific 2D case, $\rho^*(-\mathbf{r})$ corresponds to a 180° rotation of $\rho(\mathbf{r})$ with phases of opposite sign. However, they can be distinguished by considering the optical path length inside the sample. Indeed, the waves scattered by atoms at the surface and inside the wire travel along different optical paths because of the shape of the wire: the travel inside the crystal from the entrance to the scatterer and from the scatterer to the exit is less for atoms at surfaces. In the crystal, the refractive index n is slightly different from 1, which means that the phase velocity is not the same as in the air. For 9 keV X-rays in GaN, $n = 1 - \delta + i\beta$ with $\delta = 1.356 \times 10^{-5}$ and $\beta = 2.5 \times 10^{-7}$ (ref 23). δ and β imply a phase shift and an absorption, respectively. Thus, for a diameter of 500 nm, the phase shift between the surface and the center of the wire is around 0.3 rad, which is not negligible. By contrast, the absorption is less than 1% and will be neglected. According to the Fourier transform convention mentioned in eq 1, the plane wave of the incident and diffracted beam is written e^{ikr}, where $k = 2\pi/\lambda$ is the wave vector of the plane wave in vacuum and λ the wavelength of the X-ray beam. After a traveled distance d inside the crystal, the phase of the beam is shifted negatively by $-k\delta d$. A negative curvature of the phase is therefore expected in the middle of the wire, which is clearly identified in one of the two possible reconstructed objects (Figure 4).

Moreover, the specific fingerprint of the phase shift coming from the optical path length cannot be confused with a displacement field inside the wire. In particular, the phase is curved only in the direction transverse to the scattering plane (X), and is flat along the longitudinal one (Figure 4). Note that we neglect the curvature of the incident wavefront, which is mostly flat at this scale for our setup.[24] In conclusion, the identification of the optical path length effect allows the unambiguous determination of the correct solution $\rho(\mathbf{r})$, from which we can deduce the polarity of each domain.

Figure 3b displays the best reconstructed images of the wire for the 5 Bragg peaks including the optical path length correction. All five solutions converge to the same shape and inner structure. The average diameter of the wire is estimated at (490 ± 10) nm. The reconstructions clearly evidence the presence of

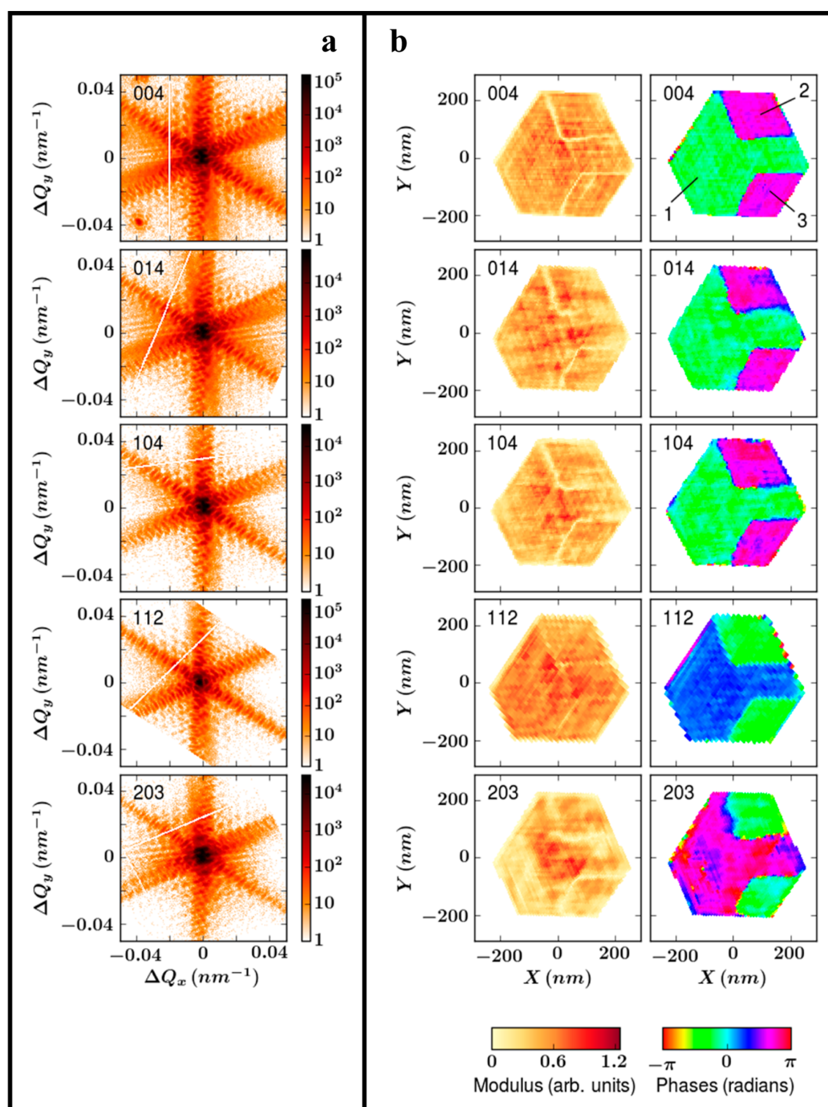

Figure 3. Coherent X-ray diffraction measurements of five Bragg reflections of a single GaN wire and the corresponding real space reconstructions (modulus and phase). The (*hkl*) planes are indicated in the top left corner of the figures. (a) Intensities are shown in counts with a log scale. (b) The real space reconstructions (modulus and phase), the (*X*,*Y*,*Z*) axis correspond to the crystallographic directions([$\bar{2}\bar{1}0$],[010],[001]).

three domains: one large and two smalls. The phase values (Figure 3b) are constant inside the domains and the two small domains show the same phase value for all reconstructions. In the following, the three domains will be called domains 1, 2, and 3 as mentioned in Figure 3b. The IDBs, separating the domains, correspond to the $\{100\}$ planes, which have been reported in many studies.[25,26] In the modulus maps of the reconstructed samples (Figure 3b), a gap clearly appears at the position of the IDBs. This is an artifact of the Fourier transform caused by data truncation. Indeed, numerical test demonstrates that an ideal sample with homogeneous modulus map and a phase shift between domains cannot be reconstructed without such an artifact, since only a small part of the reciprocal space is used for reconstruction. In the present study, the measured reciprocal space corresponds to the 20th of the reciprocal space unit cell. Such a partial reciprocal space measurement implies an artifact in the modulus of the reconstructed object.

The homogeneity of the phase inside the domains denotes the absence of significant strain variation. The first column of Table 1 reports the experimental difference in the phase values between domains 1 and 2−3 at different Bragg reflections. These differences originate in the phase difference of the structure factor ψ_F between Ga and N-terminated GaN domains and a homogeneous displacement of the domains between each other. For the calculations of ψ_F, the internal parameter u_c is equal to 0.377 (ref 27) and the analytical atomic scattering factors of Ga and N were taken from the work of Waasmaier and Kirfel.[28] This work assumes a spherical electron density around atoms, which is not perfectly true for the GaN wurtzite since the Ga−N

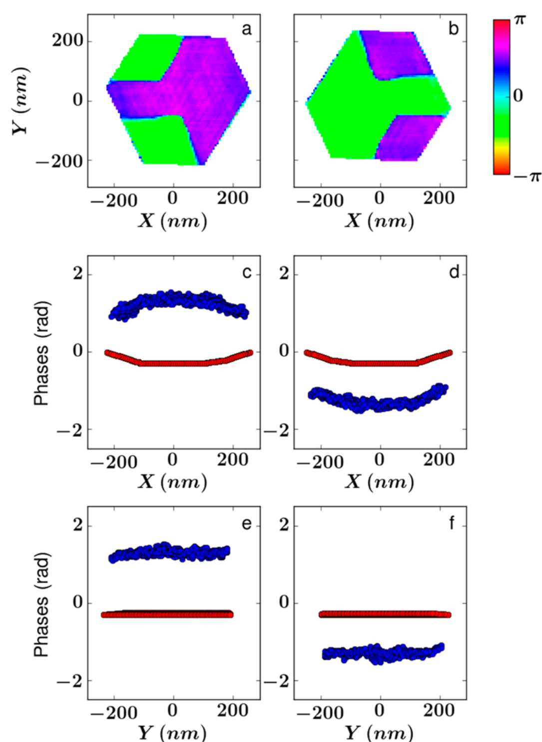

Figure 4. Effect of the optical path length. (a and b) Two phase maps of reconstructed objects giving the same 004 diffraction patterns. The phase changes along the *X* and *Y* directions in the reconstructed objects (blue dots) are compared to the expected phase changes originated in the optical path lengths (red dots): (c and e) for the solution shown in (a) and (d and f) for the solution shown in (b). This confirms solution (b) as the correct one.

TABLE 1. Phase Difference between the Domains 1 and 2−3[a]

(*hkl*)	$\Delta\phi$ experimental (rad)	$\Delta\psi$ theoretical (rad)	$\Delta\phi$ (rad) with $U_z = (c/2 + 8)$ pm and $U_{x,y} = 0$ pm
(004)	−2.80 ± 0.05	3.07	−2.79
(014)	−2.75 ± 0.1	3.07	−2.79
(104)	−2.85 ± 0.1	3.07	−2.79
(112)	1.50 ± 0.1	1.24	1.45
(203)	2.80 ± 0.2	−0.63	2.81

[a] For the two last columns, domains 1 and 2−3 are related to −*c* and +*c* GaN crystal, respectively.

bonds have a strong ionic character. However, the difference with the structure factor determined from convergent beam electron diffraction or from electron densities calculated using density functional theory does not affect ψ_F by more than a few hundredths of a radian.[29] The theoretical difference of the structure factor ($\Delta\psi_F$) between −*c* and +*c* domains are reported in the second column of Table 1, supposing that the 1 and 2−3 domains are −*c* and +*c* oriented, respectively. It clearly shows a disagreement with experimental values. One has to introduce a rigid displacement of the atomic lattice in the *z* direction of (*c*/2 + 8) pm of the +*c* with respect to the −*c* domains (see third column of Table 1) to match the experimental values. The error bar of this value is estimated to be 1 pm from the accuracy of the phase shift. The theoretical values do not fit the experimental ones, when the polarities of the 1 and 2−3 domains are mutually exchanged, meaning that the 1 and 2−3 domains are +*c* (Ga-terminated) and −*c* (N-terminated) oriented crystals, respectively. Thus, it is possible to assert that the largest domain is −*c* (N-terminated) and the two small domains are +*c* (Ga-terminated), in agreement with the usual tendency of this type of wire growth.[5,20] Moreover, the displacement of the atomic lattice between the −*c* and +*c* inversion domains along the *z* direction implies that the Ga atomic network of the +*c* domains is 8 pm higher than the N atomic network of the −*c* domain. In the (*x*,*y*)-plane, no displacement is needed to fit the experimental phase values. Nevertheless, the accuracy of the displacement in this plane is worse than the one along the *z* axis. It is estimated to 4 pm. This implies that atoms from domains 2−3 are shifted by less than 4 pm in the (*x*,*y*)-plane with respect to the atoms of domain 1.

Four different models of the {100}, IDB structure have been reported in the literature.[30,31] One of them, the IDB* structure proposed by Northurp *et al.*,[30] is by far the best match with our measurements. It can be formed by translating one side of an IDB by *c*/2 along the [001] direction and contains 4-fold and 8-fold rings of bonds that prevent Ga−Ga and N−N bonds. It has been demonstrated that the IDB* structure is the most energetically favorable one and the one experimentally observed in thin films.[26] However, the IDB* structure differs from our results in two ways. On the one hand, the displacement along the *z* axis is *c*/2 for the IDB* and our measurements in the GaN wire reveal an additional shift of +8 pm. On the other hand, the 10 pm displacement perpendicular to the IDB* predicted by Northrup *et al.* is not observed in our wire. However, it can be noted that this experimental work corresponds to a more complicated situation: this wire contains several IDBs* which interact with each other and with the surfaces. Such a configuration can affect the equilibrium structure of the IDB*, which has been calculated for an isolated defect in an infinite media by Northrup and coworker.[30] Moreover, in a wire containing several IDBs* with different orientations, the displacements perpendicular to the IDBs* have to relax to accommodate each other. Interestingly, our molecular statics calculations with Tersoff-Brenner potential failed to reproduce the displacement field found experimentally, even though the complex configuration of domains had been taken into account (Supporting Information S3).

It is worth noting that the 004 reflection has been measured at mid-height of several GaN wires (see Supporting Information S2). Different domain configurations were observed, but the retrieved phase shift between inversion domains is always the same.

ARTICLE

Therefore, we conclude that the 8 pm displacement along the *c*-axis, determined with an accuracy of 1 pm, is not due to a particular domain configuration, but a general feature of the IDB* structure. The in-plane components of the displacement field were measured only for the wire of Figure 3, which suggests that the in-plane components must be smaller than the accuracy of our measurements in that plane (~4 pm).

A possible explanation, yet to be verified, to the discrepancy between experimental and numerical results, is the segregation of silicon atoms in the IDBs. Indeed, the growth is performed with a high Si-dopant concentration (above 10^{20} cm^{-3} in the wire bulk[16]), and it is known that the presence of silicon at an IDB perpendicular to the *c*-axis modifies the bond length at the interface.[32] The present case of these prismatic IDBs has not been reported yet.

CONCLUSIONS

In conclusion, the inner structure of GaN wires containing a complex arrangement of inversion domains has been investigated by CBI with a spatial resolution of 6 nm and a displacement field accuracy of 1 pm along the *c*-axis and 4 pm in the (001) plane. The absolute polarity of the domains is unambiguously revealed and the microscopic structures of the IDBs characterized: the Ga-terminated domains undergo a rigid relative displacement with respect to the N-terminated domain of ($c/2 + 8$) pm along the *c*-axis and almost zero in the (001) plane. Such a surprising displacement field cannot be explained by atomistic simulations and may originate in the high Si-dopant concentration. Finally, let us point out that this study demonstrates that the CBI technique offers the possibility to get a very precise inner view of the microstructure of small crystals in the presence of interacting defects. This work opens the way to the nondestructive characterization of various defects inside small crystals. This technique can be also applied in a straightforward manner to materials under complex environment or *operando* as found in microelectronics and optoelectronics devices.

METHODS

Sample Preparation. The growth of self-catalyzed GaN wires has been performed on *c*-plane sapphire substrates by metal organic vapor phase epitaxy (MOVPE) in a 3 × 2 in. closed-coupled showerhead reactor. As described by R. Koester *et al.*,[16] the substrate is cleaned under H_2 at high temperature and annealed under ammonia to promote the formation of an Al(O)N layer (~1.5 nm thick according to X-ray reflectivity measurement) before the deposition of a thin SiN_x layer (~2 nm thick) playing the role of a selective growth layer with respect to GaN.[33] Another ammonia annealing stabilizes the surface stoichiometry and induces the formation of composition fluctuations or thinner areas that can be punched through by GaN deposition to achieve epitaxy with sapphire. The GaN polarity and the shape of the objects are directly determined by the atomic stacking of the Al(O)N layer.[25] A high Si-dopant concentration (induced by silane diluted in a majority N_2 carrier gas) and a small V/III molar ratio (ammonia to trimethylgallium) promote the vertical wire growth (see details in ref 16). By adjusting the growth conditions for CBI studies, we obtained 3−5 μm wire length for 150 s of growth with quite low density (about 10^6 cm^{-2}) as illustrated by the scanning electron microscopy view of Figure 1a.

Experiment. X-ray Coherent Bragg Imaging was performed at the ID01 beamline of the European Synchrotron Radiation Facility. A coherent portion of the monochromatic (9.0 keV) beam was selected with high precision slits by matching their horizontal and vertical gaps with the transverse coherence lengths of the beamline: 20 μm (horizontally) and 60 μm (vertically) close to the sample position. The coherent beam was then focused to 0.8 μm × 0.4 μm using a Fresnel Zone Plate (diameter of 300 μm), in order to illuminate a single GaN wire (Figure 2). Diffraction was measured by a two-dimensional detector (516 × 516 pixels of 55 μm placed at 1.307 m from the sample). 3D data sets were recorded by rocking the sample over a range of 1.28° by steps of 0.005°.

Reconstruction. Three standard algorithms were used: Error Reduction (ER), Hybrid Input-Output (HIO) and Shrink Wrap (SW).[21,22] At each step, constraints are applied in the reciprocal space and in the direct space. A custom version of the SW method has been used to determine the support region, *i.e.*, the shape of the object. The SW procedure is stopped when the shrinking process slows down. The support or shape of the object is then adapted manually to get the best homogeneous modulus map. With these supports, a procedure mixing ER and HIO is done 1000 times with different initial random phases associated with the measured intensity. The modulus was left completely free inside the support.

Conflict of Interest: The authors declare no competing financial interest.

Supporting Information Available: The Supporting Information is available free of charge on the ACS Publications website at DOI: 10.1021/acsnano.5b03857.

Additional information on the reconstruction process, the measurements on other wires and molecular statics simulations (PDF)

Acknowledgment. The authors are grateful to ESRF for allocating beamtime on the ID01 beamline. This work has been funded by the French National Research Agency through the project ANR-11-BS10-01401 MecaniX. All the authors took part in the X-ray experiments. O.T. supervised the project. The paper was written by S.L., M.-I.R., G.B., J.E., M.G. and O.T. J.E. prepared the wires. S.L conducted the phase retrieval in collaboration with M.-I.R., G.B., and M.D. S.L., G.B., and M.G carried out the analysis. F.M. helped with the wavefront calculation. M.G. conducted the molecular static calculations.

REFERENCES AND NOTES

1. Yu, P. Y.; Cardona, M. *Fundamentals of Semiconductors—Physics and Materials Properties*, 4th ed.; Springer: Berlin, 2010.
2. Hirsch, P.; Horne, R.; Whelan, M. Direct Observations of the Arrangement and Motion of Dislocations in Aluminium. *Philos. Mag.* **1956**, *1*, 677–684.
3. Bourret, A.; Desseaux, J. Dislocations at Atomic Scale. *Nature* **1978**, *272*, 151–152.
4. Hytch, M. J.; Putaux, J.-L.; Pénisson, J.-M. Measurement of the Displacement Field of Dislocations to 0.03 Å by Electron Microscopy. *Nature* **2003**, *423*, 270–273.
5. Chen, X. J.; Hwang, J.-S.; Perillat-Merceroz, G.; Landis, S.; Martin, B.; Le Si Dang, D.; Eymery, J.; Durand, C. Wafer-Scale Selective Area Growth of GaN Hexagonal Prismatic Nanostructures on c-Sapphire Substrate. *J. Cryst. Growth* **2011**, *322*, 15–22.

6. Tessarek, C.; Bashouti, M.; Heilmann, M.; Dieker, C.; Knoke, I.; Spiecker, E.; Christiansen, S. Controlling Morphology and Optical Properties of Self-Catalyzed, Mask-Free GaN Rods and Nanorods by Metal-Organic Vapor Phase Epitaxy. *J. Appl. Phys.* **2013**, *114*, 144304.
7. Pfeifer, M. A.; Williams, G. J.; Vartanyants, I. A.; Harder, R.; Robinson, I. K. Three-Dimensional Mapping of a Deformation Field Inside a Nanocrystal. *Nature* **2006**, *442*, 63–66.
8. Newton, M. C.; Leake, S. J.; Harder, R.; Robinson, I. K. Three-Dimensional Imaging of Strain in a Single ZnO Nanorod. *Nat. Mater.* **2010**, *9*, 120–124.
9. Yang, W.; Huang, X.; Harder, R.; Clark, J. N.; Robinson, I. K.; Mao, H.-K. Coherent Diffraction Imaging of Nanoscale Strain Evolution in a Single Crystal Under High Pressure. *Nat. Commun.* **2013**, *4*, 1680.
10. Cha, W.; Jeong, N. C.; Song, S.; Park, H.-J.; Pham, T. C.P.; Harder, R.; Lim, B.; Xiong, G.; Ahn, D.; McNulty, I.; et al. Core−Shell Strain Structure of Zeolite Microcrystals. *Nat. Mater.* **2013**, *12*, 729–734.
11. Takahashi, Y.; Suzuki, A.; Furutaku, S.; Yamauchi, K.; Kohmura, Y.; Ishikawa, T. Bragg X-Ray Ptychography of a Silicon Crystal: Visualization of the Dislocation Strain Field and the Production of a Vortex Beam. *Phys. Rev. B: Condens. Matter Mater. Phys.* **2013**, *87*, 121201(R).
12. Clark, J. N.; Ihli, J.; Schenk, A. S.; Kim, Y.-Y.; Kulak, A.; Campbell, J. M.; Nisbet, G.; Meldrum, F. C.; Robinson, I. K. Three-Dimensional Imaging of Dislocation Propagation during Crystal Growth and Dissolution. *Nat. Mater.* **2015**, *14*, 780–784.
13. Ulvestad, A.; Clark, J. N.; Harder, R.; Robinson, I. K.; Shpyrko, O. G. 3D Imaging of Twin Domain Defects in Gold Nanoparticles. *Nano Lett.* **2015**, *15*, 4066–4070.
14. Nakamura, S.; Senoh, M.; Iwasa, N.; Nagahama, S. High-Brightness InGaN Blue, Green and Yellow Light-Emitting Diodes with Quantum Well Structures. *Jpn. J. Appl. Phys.* **1995**, *34*, L797–L799.
15. Kirste, R.; Collazo, R.; Callsen, G.; Wagner, M. R.; Kure, T.; Reparaz, J. S.; Mita, S.; Xie, J.; Rice, A.; Tweedie, J.; et al. Temperature Dependent Photoluminescence of Lateral Polarity Junctions of Metal Organic Chemical Vapor Deposition Grown GaN. *J. Appl. Phys.* **2011**, *110*, 093503.
16. Koester, R.; Hwang, J. S.; Durand, C.; Le Si Dang, D.; Eymery, J. Self-Assembled Growth of Catalyst-Free GaN Wires by MOVPE. *Nanotechnology* **2010**, *21*, 015602.
17. Hersee, S. D.; Sun, X. Y.; Wang, X. The Controlled Growth of GaN Nanowires. *Nano Lett.* **2006**, *6*, 1808–1811.
18. Coulon, P. M.; Mexis, M.; Teisseire, M.; Jublot, M.; Vennéguès, P.; Leroux, M.; Zuniga-Perez, J. Dual-Polarity GaN Micropillars Grown by Metal Organic Vapour Phase Epitaxy: Cross-Correlation between Structural and Optical Properties. *J. Appl. Phys.* **2014**, *115*, 153504.
19. Chen, X. J.; Perillat-Merceroz, G.; Sam-Giao, D.; Durand, C.; Eymery, J. Homoepitaxial Growth of Catalyst-Free GaN Wires on N-polar Substrates. *Appl. Phys. Lett.* **2010**, *97*, 151909.
20. Alloing, B.; Vézian, S.; Tottereau, O.; Vennéguès, P.; Beraudo, E.; Zuniga-Perez, J. On the Polarity of GaN Micro- and Nanowires Epitaxially Grown on Sapphire (0001) and Si (111) Substrates by Metal Organic Vapor Phase Epitaxy and Ammonia-Molecular Beam Epitaxy. *Appl. Phys. Lett.* **2011**, *98*, 011914.
21. Fienup, J. R. Phase Retrieval Algorithms: a Comparison. *Appl. Opt.* **1982**, *21*, 2758–2769.
22. Marchesini, S. X-Ray Image Reconstruction from a Diffraction Pattern Alone. *Phys. Rev. B: Condens. Matter Mater. Phys.* **2003**, *68*, 140101.
23. Henke, B. L.; Gullikson, E. M.; Davis, J. C. X-Ray Interactions: Photoabsorption, Scattering, Transmission, and Reflection at E = 50−30000 eV, Z = 1−92. *At. Data Nucl. Data Tables* **1993**, *54*, 181–342.
24. Mastropietro, F.; Carbone, D.; Diaz, A.; Eymery, J.; Sentenac, A.; Metzger, T. H.; Chamard, V.; Favre-Nicolin, V. Coherent X-Ray Wave Front Reconstruction of a Partially Illuminated Fresnel Zone Plate. *Opt. Express* **2011**, *19*, 19223–19232.
25. Liu, F. D.; Collazo, R.; Mita, S.; Sitar, Z.; Duscher, G.; Pennycook, S. J. The Mechanism for Polarity Inversion of GaN *via* a Thin AlN Layer: Direct Experimental Evidence. *Appl. Phys. Lett.* **2007**, *91*, 203115.
26. Liu, F. D.; Collazo, R.; Mita, S.; Sitar, Z.; Pennycook, S. J.; Duscher, G. Direct Observation of Inversion Domain Boundaries of GaN on c-Sapphire at Sub-Ångstrom Resolution. *Adv. Mater.* **2008**, *20*, 2162–2165.
27. Schulz, H.; Thiemann, K. H. Crystal Structure Refinement of AlN and GaN. *Solid State Commun.* **1977**, *23*, 815–819.
28. Waasmaier, D.; Kirfel, A. New Analytical Scattering-Factor Functions for Free Atoms and Ions. *Acta Crystallogr., Sect. A: Found. Crystallogr.* **1995**, *51*, 416–431.
29. Jiang, B.; Zuo, J. M.; Holec, D.; Humphreys, C. J.; Spackman, M.; Spence, J. C. H. Combined Structure-Factor Phase Measurement and Theoretical Calculations for Mapping of Chemical Bonds in GaN. *Acta Crystallogr., Sect. A: Found. Crystallogr.* **2010**, *66*, 446–450.
30. Northrup, J. E.; Neugebauer, J.; Romano, L. T. Inversion Domain and Stacking Mismatch Boundaries in GaN. *Phys. Rev. Lett.* **1996**, *77*, 103–106.
31. Moon, W. H.; Choi, C. H. Molecular Dynamics Study of Inversion Domain Boundary in W-GaN. *Phys. Lett. A* **2006**, *352*, 538–542.
32. Liu, Z.; Wang, R.-Z.; Liu, L.-M.; Yan, H.; Lau, W.-M. Si Doping at GaN Inversion Domain Boundaries: an Interfacial Polar Field for Electron and Hole Separation. *J. Mater. Chem. A* **2014**, *2*, 9744–9750.
33. Gibart, P. Metal Organic Vapour Phase Epitaxy of GaN and Lateral Overgrowth. *Rep. Prog. Phys.* **2004**, *67*, 667–715.